Turbulent-Flow Calculations for Flow over Wings near Maximum Lift

J. E. Deese* and R. K. Agarwal†
McDonnell Douglas Research Laboratories, St. Louis, Missouri 63166

The calculation of horizontal stabilizer flowfields near maximum lift using a three-dimensional Navier-Stokes code is described. Results are presented for two stabilizer configurations with and without elevator deflection. Predicted lift coefficients are within 10% of experimental values up to the onset of stall. The code is able to predict the onset of both wing and elevator stall for the two configurations studied. Surface pressure distribution predictions are in good agreement with experimental data.

Nomenclature

b = wing semispan
C_L = wing lift coefficient
C_P = pressure coefficient, $=(P-P_\infty)/(\frac{1}{2}\rho_\infty V_\infty^2)$
$\bar{c}$ = mean aerodynamic chord length
c' = local chord length
c'_e = local elevator chord length
M = Mach number
P = pressure
Re = Reynolds number, $=(\rho_\infty V_\infty \bar{c})/\mu_\infty$
V = velocity magnitude
x = distance in chordwise direction
y = distance normal to wing surface
y^+ = law of the wall coordinate, $=(y\sqrt{\tau_w \rho})/\mu$
z = distance in spanwise direction
α = angle of attack
α_{max} = angle of attack at which wing stall occurred experimentally
δ_e = elevator deflection angle
$\delta_{e_{max}}$ = elevator deflection angle at which elevator stall occurred experimentally
μ = coefficient of viscosity
ρ = density
τ = shear stress

Subscripts

e = elevator
w = wall value
∞ = freestream value

Introduction

THE design of efficient aircraft horizontal stabilizers requires that sufficient tail forces be developed while holding the area and weight of the tail plane to a minimum. In some regions of an aircraft's operating envelope, an efficient horizontal stabilizer will be very near its maximum lift condition. A reliable, versatile, and accurate prediction method for flow over wings near their maximum lift would be a beneficial tool in the aircraft development process. Such a method would allow designers to achieve their design goals in a more timely and cost-effective manner through the reduction of expensive wind-tunnel testing.

Presented as Paper 89-2239 of the AIAA 7th Applied Aerodynamics Conference, Seattle, WA, July 31–Aug. 2, 1989; received Aug. 23, 1989; revision received May 10, 1990; accepted for publication June 13, 1990.

*Senior Scientist. Member AIAA.
†Principal Scientist. Associate Fellow AIAA.

Recent progress in computational fluid dynamics has increased the role these methods play in aircraft design. Larger and faster computers coupled with more efficient algorithms allow more sophisticated fluid flow models to be analyzed over increasingly complex configurations. Potential equation solutions have been incorporated into aircraft design procedures for some time. Euler equation solution methods for complete aircraft are now available and are being integrated into aircraft design. The more complex Navier-Stokes solvers for complete aircraft are currently in the research and development stage; they are limited by very large computer run time and memory requirements.

Although Navier-Stokes solvers are not yet practical tools for the design of complete aircraft configurations, they can be useful in analyzing aircraft components under conditions where viscous effects play a key role in determining performance. One such situation is encountered predicting wing performance near maximum lift. This paper describes the application of a Reynolds-averaged Navier-Stokes solver[1] to the calculation of the flow about two horizontal stabilizer configurations near maximum lift condition. Clean-wing and elevator-deflected results are presented and compared with experimental data. To be effective, the code must be able to predict accurately the C_L-α variation in the linear portion of the lift curve and the point at which the curve flattens out (onset of stall). The purpose of this work is to demonstrate that Navier-Stokes calculations can be an accurate and cost-effective tool for the prediction of horizontal stabilizer performance.

Governing Equations

The governing equations for this analysis are those comprising the thin-layer approximation to the full Reynolds-averaged, time-dependent Navier-Stokes equations in three dimensions for curvilinear coordinate systems. This set of equations is described in detail in Ref. 1 and will not be repeated here. The thin-layer approximation retains viscous terms in only one direction. The body surface is mapped onto a single plane in the computational space, and viscous terms normal to this plane are included in the calculations. For high Reynolds number turbulent flow, the dominant viscous effects are the result of diffusion normal to the body surface; the thin-layer approximation is suitable for flow about wings under those conditions. As the wing stalls and the separated flow regions on the upper surface become larger, the thin-layer approximation begins to break down.

Turbulence effects are included through the Baldwin-Lomax algebraic eddy viscosity model. The flow is assumed to be turbulent over the entire wing; there is no laminar-to-turbulent transition in the leading-edge region. No wake turbulence model is included.

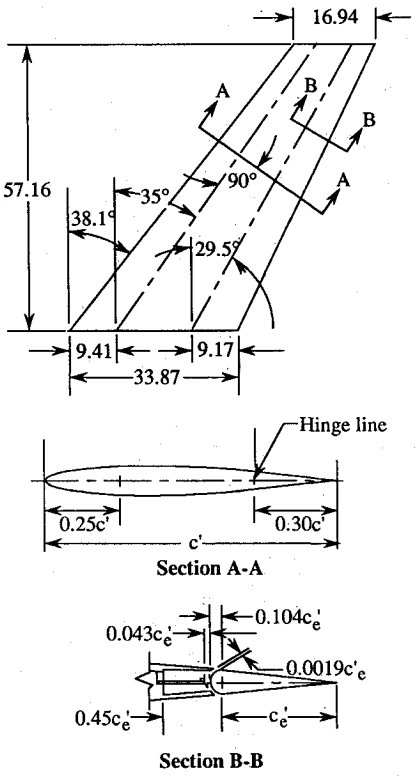

Fig. 1 Planform and cross section for the NACA horizontal tail as taken from Ref. 4.

Numerical Solution Procedure

The governing equations are solved by an explicit, fourth-order, Runge-Kutta, time-marching, finite-volume numerical scheme. A brief overview of the method will be given here; full details can be found in Ref. 1.

The thin-layer, Reynolds-averaged Navier-Stokes equations are a system of partial differential equations in space and time. Spatial and temporal terms are decoupled using the method of lines. The region surrounding a configuration is subdivided into hexahedral cells, and a system of ordinary differential equations in time is obtained by integrating over each cell volume. Flow variables are defined at cell centers, and fluxes are computed at cell faces using averages of the cell-center variables. This formulation is equivalent to a second-order-accurate, central-difference method for smooth grids.

This algorithm requires some type of numerical dissipation to prevent odd-even point decoupling and to suppress oscillations around shocks. The blended first- and third-order dissipation developed by Jameson et al.[2] is employed in these calculations. Only the third-order terms are included since the flowfields are totally subsonic.

Results

Calculations have been performed for two configurations. The first is an aspect ratio 4.5 wing tested in the wind tunnel by the National Advisory Committee on Aeronautics (NACA).[3,4] The second is a generic horizontal tail configuration tested by Douglas Aircraft Company.

NACA Wing

Figure 1, taken from Ref. 4, shows the planform and airfoil section of a horizontal stabilizer tested by NACA. The wing has an aspect ratio of 4.5, taper ratio of 0.5, and quarter-chord sweep of 35 deg. The thickness distribution normal to the quarter-chord line is that corresponding to the NACA 64A010 airfoil. Tests were performed at Mach numbers from 0.2 to 0.94, Reynolds numbers based on the mean aerodynamic chord $\bar{c}$ from 2×10^6 to 11×10^6, angles of attack from -29.0 to 29.0 deg, and elevator deflections from $+6.0$ to -25.0 deg.

The calculations presented in this paper for the NACA wing are all at a Mach number of 0.21 and a Reynolds number of 3×10^6. Elevator deflections are 0 deg and -10 deg, where a negative deflection produces a downward force on the tail. The angle of attack ranges from 0.0 to -28.0 deg in 4-deg increments. Negative angle of attack also produces a downward tail force, which will be defined as negative lift in the following discussion. Production of sufficient downward tail force is usually the critical requirement for horizontal tails.

A $160\times28\times32$ cell grid was generated by the three-dimensional code of Chen et al.[5] There are 96 cells on the wing in the chordwise direction and 24 in the spanwise direction. Figures 2 show the grid distribution at the wing root cross section and on the wing planform for the case of no elevator deflection. The value $y^+ < 5$ at the center of all cells adjacent to the wing. The cell size ratio moving away from the wing in

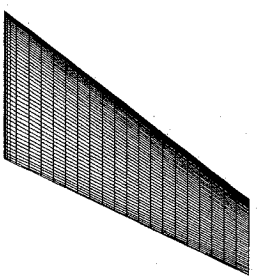

a) Planform

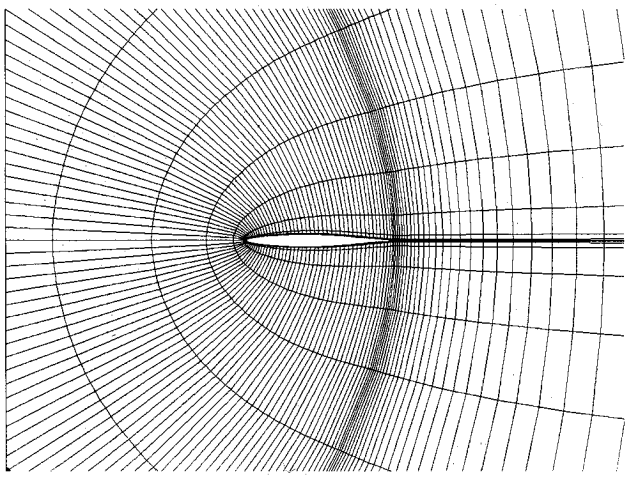

b) Cross section

Fig. 2 Planform and cross-section grid distribution for the NACA horizontal tail.

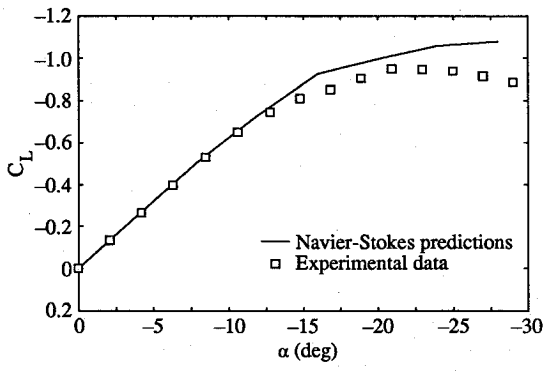

Fig. 3 Lift curve for the NACA horizontal tail: $M_\infty = 0.21$, $Re = 3\times10^6$, $\delta_e = 0.0$ deg.

the normal direction is required to be < 2. Approximately 12 cells are included in the boundary layer.

Navier-Stokes predictions for the NACA tail lift are compared with experimental data in Fig. 3. Between 0.0 and -12.0 deg the code matches the experimental lift coefficient almost exactly. For angles of attack < -12.0 deg, lift coefficient predictions are somewhat larger in magnitude than the experimental values, although the trend is correct.

The differences between the Navier-Stokes predictions and experimental data for angles of attack < -12.0 deg are a result of the inability of the code to compute separated flow properly. Three-dimensional separation is a complex phenomenon that is not quantified easily. In this analysis, the relatively simple criterion of negative chordwise velocity in a wing-adjacent cell is employed to determine the extent of separation.

Using this criterion, the code predicts no separation from $\alpha = 0.0$ through -8.0 deg. As the angle of attack decreases to $\alpha = -12.0$ deg, a significant separated flow region appears on the outboard region of the tail lower surface. Figures 4 illustrate the inboard progression of the separated flow region as the angle of attack decreases. These figures display the wing planform with dimensions normalized by $\bar{c}$. The dashed lines on the planform indicate the most forward point with a negative chordwise velocity at each span location. As the angle of attack decreases from -12.0 to -24.0 deg the separated flow region increases to encompass the majority of the tail lower surface.

Flow separation has a pronounced effect on the wing surface pressure distribution. At $\alpha = -8.0$ deg the code predictions match the measured surface pressure coefficients almost exactly, as illustrated in Fig. 5 for the midplane of the

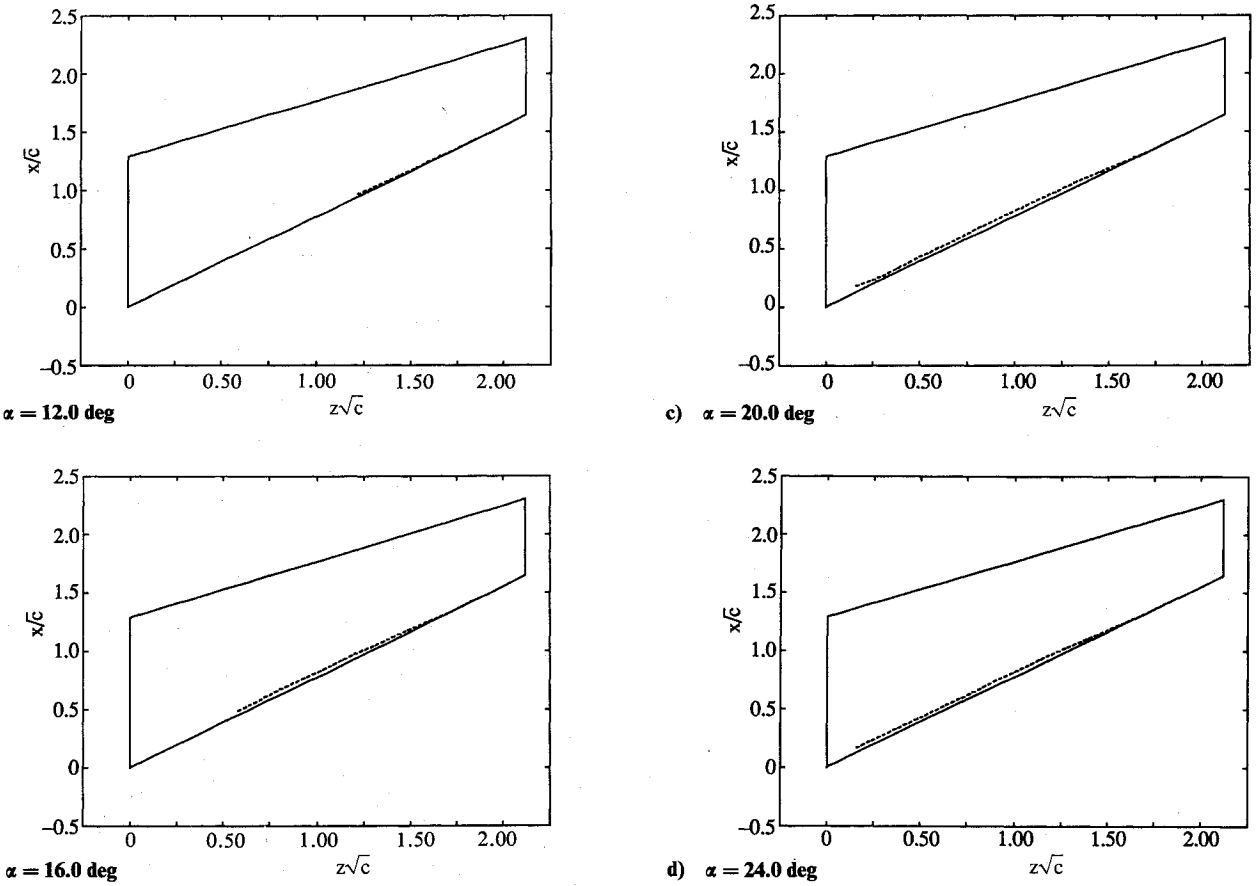

Fig. 4 Flow separation line on the NACA horizontal tail lower surface: $M_\infty = 0.21$, $Re = 3 \times 10^6$, $\delta_e = 0.0$ deg.

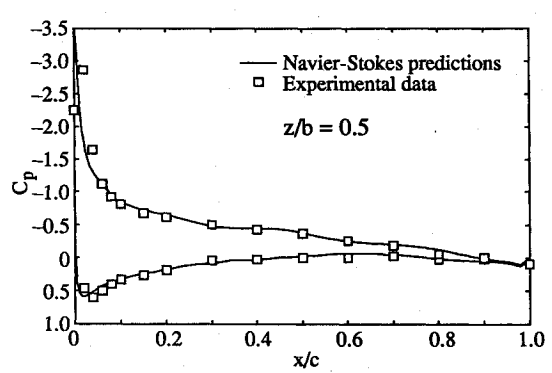

Fig. 5 Surface pressure distribution on the NACA horizontal tail: $M_\infty = 0.21$, $Re = 3 \times 10^6$, $\alpha = -8.0$ deg, $\delta_e = 0.0$ deg.

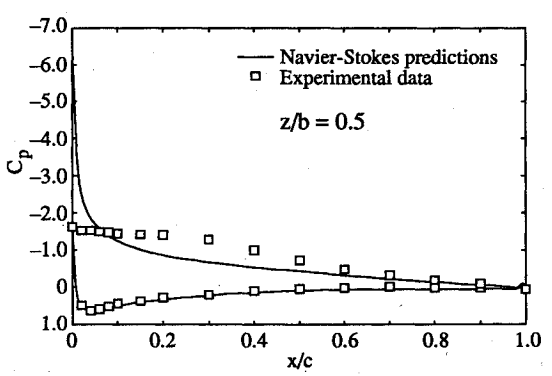

Fig. 6 Surface pressure distribution on the NACA horizontal tail: $M_\infty = 0.21$, $Re = 3 \times 10^6$, $\alpha = -12.0$ deg, $\delta_e = 0.0$ deg.

tail. Decreasing the angle of attack to −12.0 deg causes the predicted separation region to approach the midplane (Fig. 4). Comparing the predicted and experimental surface pressure distributions at $\alpha = -12.0$ deg reveals significant differences, particularly near the leading edge. Figure 6 shows the Navier-Stokes calculations to have a large suction peak consistent with attached flow at this span station. The experimental data have no suction peak and are consistent with a flow that has separated at the leading edge. At $\alpha = -20.0$ deg, both the predicted and experimental surface pressure distributions, displayed in Fig. 7, are consistent with separated flow, although they differ significantly.

These results suggest that the current implementation of the thin-layer Navier-Stokes code does an excellent job of predicting the lift curve up to the onset of stall, which is well manifested by the appearance of reverse flow. When significant separated flow is present, the code is not able to predict the flowfield accurately.

Wing behavior in the stall region can be highly dependent on the boundary-layer transition characteristics in the leading-edge region.[6] Since the current version of the Navier-Stokes code assumes fully turbulent flow over the entire wing surface, one would not expect the method to give good results when transition is important. Implementation of a laminar-to-turbulent transition model is necessary to improve the post-stall flow calculations.

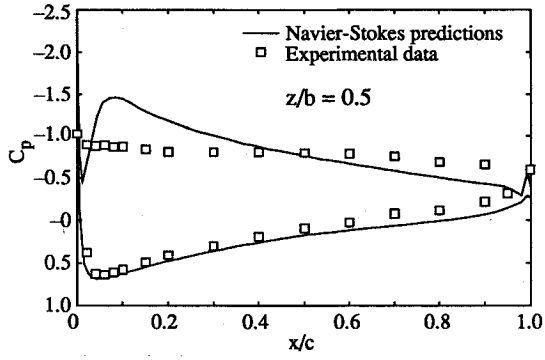

Fig. 7 Surface pressure distribution on the NACA horizontal tail: $M_\infty = 0.21$, $Re = 3 \times 10^6$, $\alpha = -20.0$ deg, $\delta_e = 0.0$ deg.

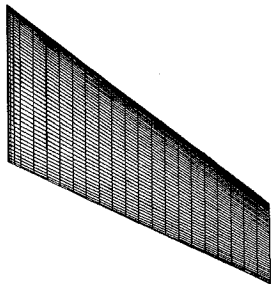

a) Planform

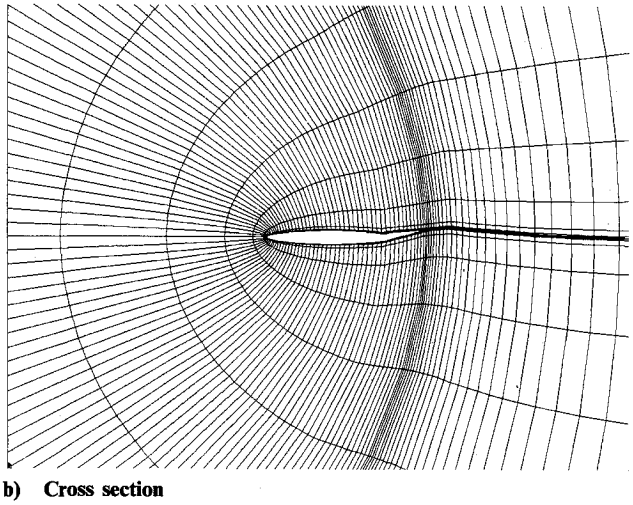

b) Cross section

Fig. 8 Planform and cross-section grid distribution for the NACA horizontal tail with elevator deflection.

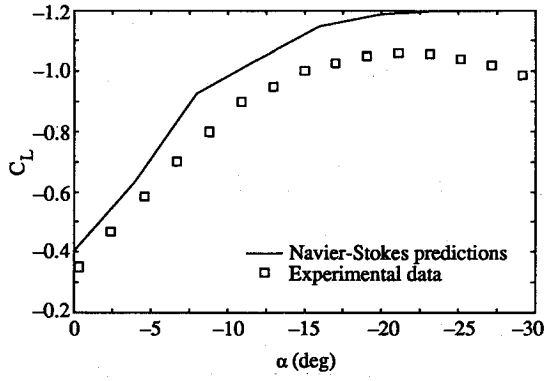

Fig. 9 Lift curve for the NACA horizontal tail: $M_\infty = 0.21$, $Re = 3 \times 10^6$, $\delta_e = -10.0$ deg.

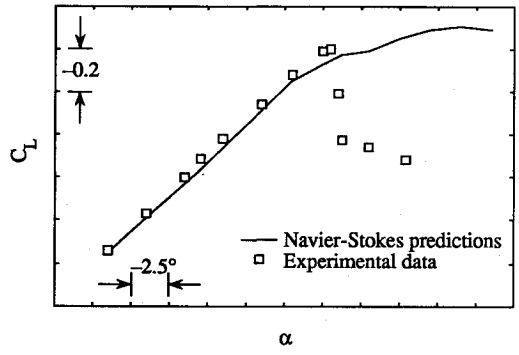

Fig. 10 Generic horizontal tail lift curve: $M_\infty = 0.215$, $Re = 1.0 \times 10^7$, $\delta_e = 0.0$ deg.

NACA Wing $\delta_e = -10.0$ deg

The grid distribution in a spanwise plane and on the surface of the NACA wing with an elevator deflection of $\delta_e = -10.0$ deg is shown in Figs. 8. Grid dimensions are $160 \times 28 \times 32$, with 96 cells on the wing in the chordwise direction and 24 cells in the spanwise direction. The grid was generated using the method of Ref. 5. A value of < 5 is maintained for y^+ at the surface adjacent cells. Calculations were performed at $M_\infty = 0.21$ and $Re = 3 \times 10^6$.

Figure 9 compares the predicted and measured lift curves for this configuration. The code consistently overpredicts the magnitude of the lift by about 10%. As the tail begins to stall, the predictions become less accurate in a manner similar to the clean-wing case previously discussed. Separation first occurs in the leading-edge region around $\alpha = -12.0$ deg and moves inboard in a manner similar to that observed for the $\delta_e = 0.0$ deg case.

Generic Horizontal Tail

Calculations have been performed for a generic horizontal tail tested by Douglas Aircraft Company.[7] A $160 \times 28 \times 32$ cell grid analogous to that shown in Fig. 2 for the NACA tail was generated using the method of Chen et al.[5] At the center of all cells adjacent to the wing surface, $y^+ < 5$. All calculations for this wing are at $M_\infty = 0.215$ and $Re = 1.0 \times 10^7$.

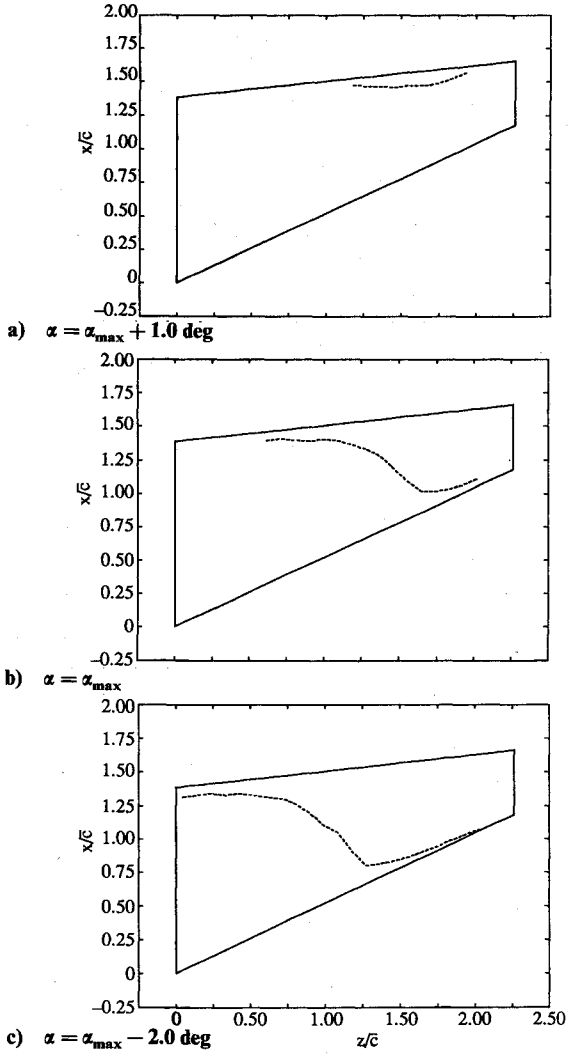

Fig. 11 Flow separation on the generic horizontal stabilizer lower surface: $M_\infty = 0.215$, $Re = 1.0 \times 10^7$, $\delta_e = 0.0$ deg.

Figure 10 compares the lift curve predicted by the Navier-Stokes method with experimental data. In Fig. 10, the angle of attack is decreasing from left to right and the lift coefficient is decreasing from bottom to top. For a range of α down to α_{max}, the predicted C_L curve is within 5% of the experimental curve.

At angles less (more negative) than α_{max} a very sharp stall was observed experimentally with flow separation occurring initially at about 70% span and spreading rapidly inboard. The Navier-Stokes code predicts a leveling of the lift curve in the α_{max} region, a further decrease in C_L at lower angle of attack, and stall at about $\alpha_{max} - 7$ deg. Only the linear region of the horizontal tail lift curve is useful for aircraft control, and so for design purposes the code predicts the same limit of tail effectiveness as was observed experimentally.

Using the negative chordwise velocity criterion, flow separation is first predicted along the wing trailing edge at $\alpha_{max} + 1$ deg, as shown in Fig. 11a. At α_{max}, separation has spread forward in the 70–80% span region to a point near the leading edge, as illustrated in Fig. 11b. Some loss of downward force in the region of separation accounts for the leveling of the predicted lift curve in the α_{max} region. Figure 11c shows that the region of separation does not move inboard very rapidly at lower angles of attack. Decreasing lift at inboard span stations as α decreases allows the calculated wing lift coefficient to decrease until α reaches $\alpha_{max} - 7$ deg. Experimental data show that the flow separation region moved inboard almost immediately as the angle of attack decreased below α_{max}, causing a sharp stall.

Prior to stall, the code does an excellent job of predicting surface pressure distributions as well as lift coefficients. Figures 12 show a comparison of the predicted surface pressure coefficients with experimental data at four span stations for an angle of attack of $\alpha_{max} + 3$ deg. Agreement is excellent except near the leading edge, where the code tends to underpredict the suction peak.

Generic Horizontal Tail with Elevator Deflection

Generic horizontal stabilizer calculations have been performed at two elevator deflections, $\delta_{e_{max}} + 6$ deg and $\delta_{e_{max}}$, where $\delta_{e_{max}}$ is a reference elevator deflection angle. Experi-

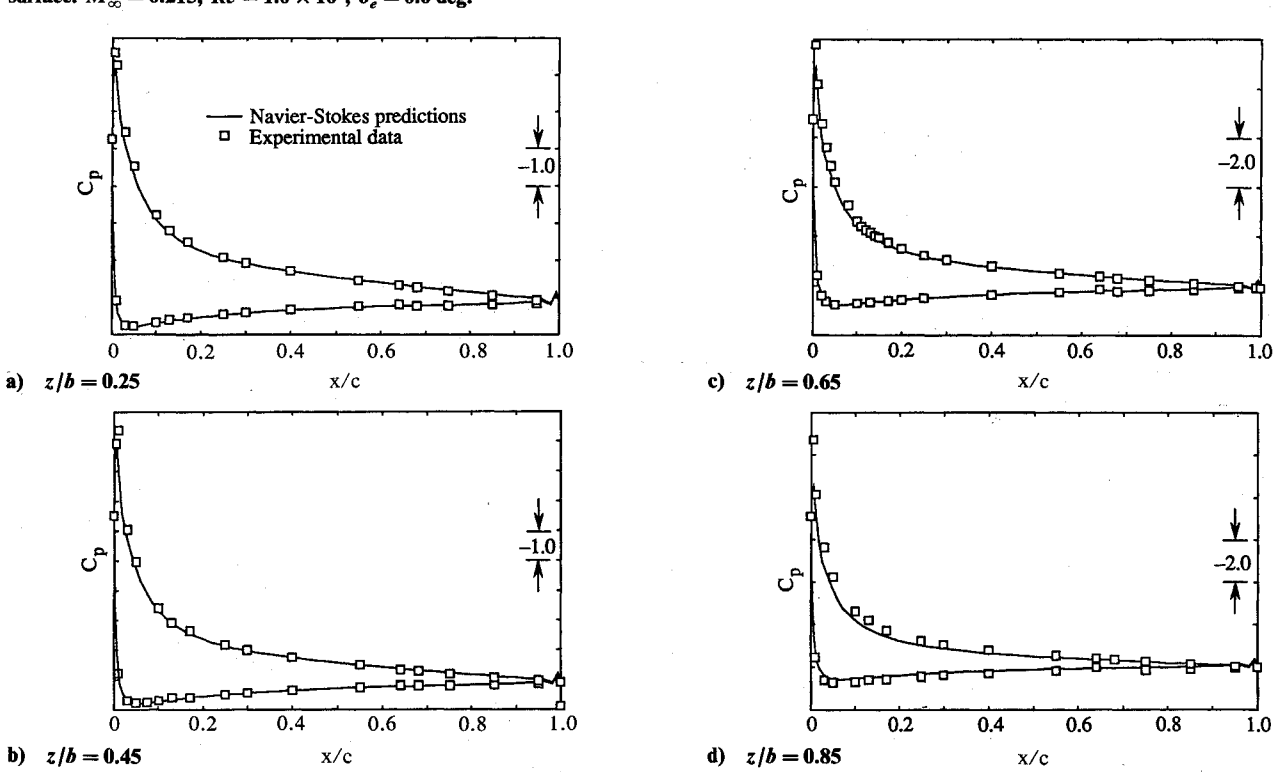

Fig. 12 Surface pressure distribution on the generic horizontal stabilizer: $M_\infty = 0.215$, $Re = 1.0 \times 10^7$, $\alpha = \alpha_{max} + 3.0$ deg, $\delta_e = 0.0$ deg.

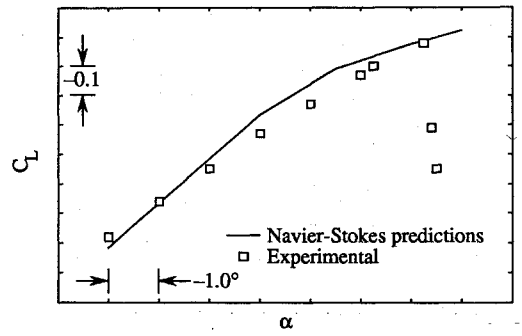

Fig. 13 Lift curve for the generic horizontal tail: $M_\infty = 0.215$, $Re = 1.0 \times 10^7$, $\delta_e = \delta_{e\max} + 6.0$ deg.

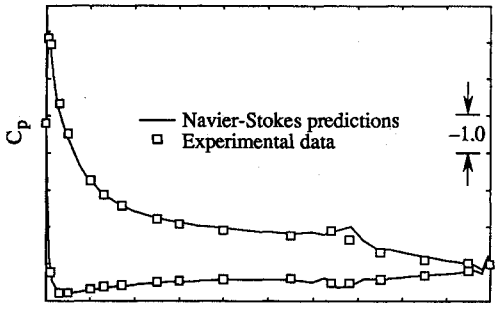

a) $z/b = 0.25$

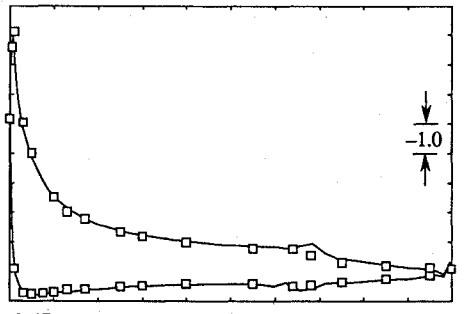

b) $z/b = 0.45$

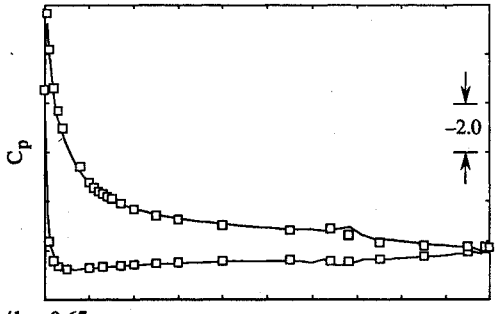

c) $z/b = 0.65$

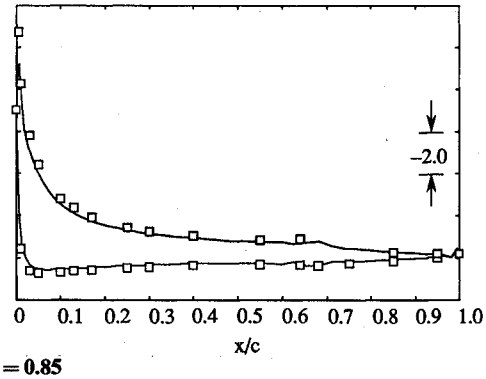

d) $z/b = 0.85$

Fig. 14 Surface pressure distribution on the horizontal stabilizer: $M_\infty = 0.215$, $Re = 1.0 \times 10^7$, $\alpha = \alpha_{\max} + 6.0$ deg, $\delta_e = \delta_{e\max} + 6.0$ deg.

mentally, the generic tail displayed the same stall characteristics with elevator deflected as it did with no deflection: a linear lift curve to the onset of stall and a precipitous decrease in downward tail force at lower angles. The code failed to predict accurately the precipitous stall, but calculated lift coefficients are within 5% of experimental values prior to stall, as shown in Fig. 13. Surface pressure distributions at $\alpha = \alpha_{\max} + 6$ deg and $\delta_e = \delta_{e\max} + 6$ deg are compared in Fig. 14. The calculated values are nearly identical to the experimental values except at the suction peak. No separated flow region appeared for this case.

Results at $\delta = \delta_{e\max}$ show trends similar to those at $\delta_{e\max} + 6$ deg. In fact, the lift curve is very close to that at $\delta_{e\max} + 6$ deg, indicating that the elevator is not effective at this deflection angle. Prior to stall, the code predictions are within 10% of experimental values, as displayed in Fig. 15. Experimentally, the wing stalls precipitously while the code predicts a more gentle behavior.

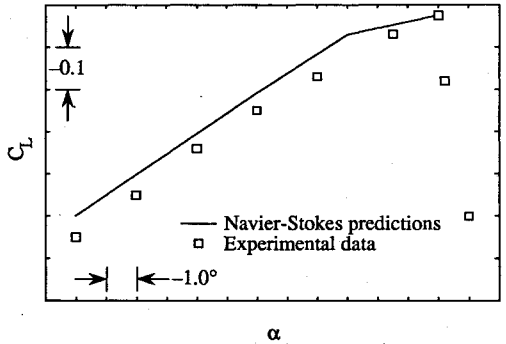

Fig. 15 Lift curve for the generic horizontal tail: $M_\infty = 0.215$, $Re = 1.0 \times 10^7$, $\delta_e = \delta_{e\max}$.

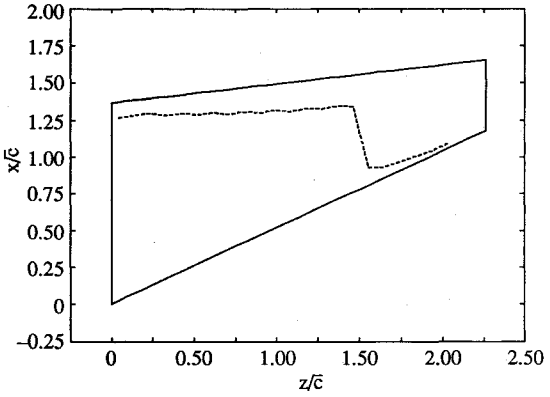

Fig. 16 Flow separation line on the lower surface of the generic horizontal stabilizer: $M_\infty = 0.215$, $Re = 1.0 \times 10^7$, $\alpha = \alpha_{\max} + 6.0$ deg, $\delta_e = \delta_{e\max}$.

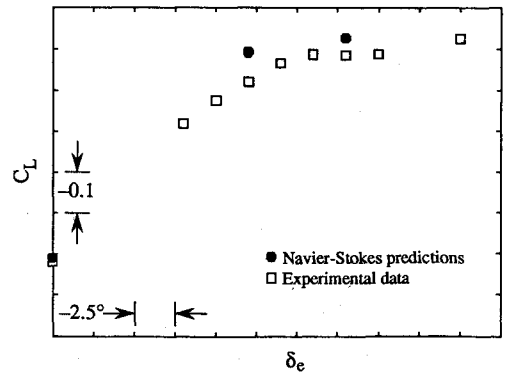

Fig. 17 Lift coefficient variation with elevator deflection for the generic horizontal tail: $M_\infty = 0.215$, $Re = 1.0 \times 10^7$, $\alpha = \alpha_{\max} + 6.0$ deg.

As δ_e decreases from $\delta_{e_{max}} + 6$ deg to $\delta_{e_{max}}$ at $\alpha = \alpha_{max} + 6$ deg, the elevator stalls and loses its effectiveness as a high-lift device. Figure 16 shows that the entire elevator is stalled at $\alpha = \alpha_{max} + 6.0$ deg and $\delta_e = \delta_{e_{max}}$. Plotting C_L vs δ_e for this angle of attack in Fig. 17 clearly illustrates the ineffectiveness of the elevator. The Navier-Stokes code correctly predicts the variation of C_L with δ_e.

Code Execution Time

The current version of the code requires 2.5×10^{-5} s per grid point per iteration on a Cray X-MP/18. For the $160 \times 28 \times 32$ cell grids used in this study, one iteration requires about 3.6 s. Typically, 2000–3000 iterations on the finest mesh are sufficient for convergence.

Conclusions

A three-dimensional, Reynolds-averaged Navier-Stokes code has been applied to the calculation of flow over horizontal tails near maximum lift. Results for two wings with and without elevator deflection show lift curve predictions within 10% of experimental values up to the onset of stall. Appearance of flow separation over some portion of the tail is an accurate criterion for determination of the onset of stall. Since the method can predict accurately the linear portion of the lift curve and the onset of stall, it is a useful tool in the evaluation of horizontal tail designs.

The code is also useful for the prediction of elevator effectiveness. For the configurations studied, the method predicted the correct variation of lift with elevator deflection through the elevator stall angle.

As the wing stalls and flow separation becomes more extensive, the code prediction becomes less accurate. Implementation of a transition model should improve calculations in the poststall region.

Acknowledgments

This research was conducted under the McDonnell Douglas Independent Research and Development program. The authors gratefully acknowledge the support of Douglas Aircraft Company for funding a portion of this work. The authors would like to thank R. W. Hoch of Douglas Aircraft Company for his assistance during this project, particularly in providing the computational grids and generic horizontal tail experimental data.

References

[1]Deese, J. E., and Agarwal, R. K., "Navier-Stokes Calculations of Transonic Flow About Wing/Body Configurations," *Journal of Aircraft*, Vol. 25, No. 12, 1988, pp. 1106–1112.

[2]Jameson, A., Schmidt, W., and Turkel, E., "Numerical Solutions of the Euler Equations by Finite Volume Methods Using Runge-Kutta Time-Stepping Schemes," AIAA Paper 81–1259, June 1981.

[3]Tinling, B. E., and Dickson, J. K., "Tests of a Model Horizontal Tail of Aspect Ratio 4.5 in the Ames 12-Foot Pressure Wind Tunnel. I. Quarter-Chord Line Swept Back 35°," NACA RM A9G13, 1949.

[4]Dods, J. B., and Tinling, B. E., "Summary of Results of a Wind-Tunnel Investigation of Nine Related Horizontal Tails," NACA TN-3497, 1955.

[5]Chen, L. T., Vassberg, J. C., and Peavey, C. C., "A Transonic Wing-Body Flowfield Calculation with Improved Grid Topology and Shock-Point Operators," AIAA Paper 84-2157, 1984.

[6]Cebeci, T., Clark, R. W., Chang, K. C., Halsey, N. D., and Lee, K., "Airfoils with Separation and the Resulting Wakes," *Journal of Fluid Mechanics*, Vol. 163, 1986, pp. 323–347.

[7]Hoch, R. W., private communication, Douglas Aircraft Company, 1988.